Acta Oceanol. Sin., 2021, Vol. 40, No. 9, P. 1–12
https://doi.org/10.1007/s13131-021-1811-5
http://www.aosocean.com
E-mail: ocean2@hyxb.org.cn

Denitrification-nitrification process in permeable coastal sediments: An investigation on the effect of salinity and nitrate availability using flow-through reactors

Shan Jiang[1, 2*], Mark Kavanagh[3], Juan Severino Pino Ibánhez[2, 4], Carlos Rocha[2]

[1] State Key Laboratory of Estuarine and Coastal Research, East China Normal University, Shanghai 200062, China

[2] School of Natural Sciences, Trinity College Dublin, Dublin 2, Ireland

[3] Trinity Centre for the Environment, School of Natural Sciences, Trinity College Dublin, Dublin 2, Ireland

[4] Instituto de Investigacións Mariñas, Consejo Superior de Investigaciones Científicas, Vigo 36208, Spain

Received 3 August 2020; accepted 13 January 2021

Abstract

Permeable coastal sediments act as a reactive node in the littoral zone, transforming nutrients via a wide range of biogeochemical reactions. Reaction rates are controlled by abiotic factors, e.g., salinity, temperature or solute concentration. Here, a series of incubation experiments, using flow-through reactors, were conducted to simulate the biogeochemical cycling of nitrate (NO_3^-) and phosphorus (P) in permeable sediments under different NO_3^- availability conditions (factor I) along a salinity gradient (admixture of river and seawater, factor II). In an oligotrophic scenario, i.e., unamended NO_3^- concentrations in both river and seawater, sediments acted as a permanent net source of NO_3^- to the water column. The peak production rate occurred at an intermediate salinity (20). Increasing NO_3^- availability in river water significantly enhanced net NO_3^- removal rates within the salinity range of 0 to 30, likely via the denitrification pathway based on the sediment microbiota composition. In this scenario, the most active removal was obtained at salinity of 10. When both river and seawater were spiked with NO_3^-, the highest removal rate switched to the highest salinity (36). It suggests the salinity preference of the NO_3^- removal pathway by local denitrifiers (e.g., *Bacillus* and *Paracoccus*) and that NO_3^- removal in coastal sediments can be significantly constrained by the dilution related NO_3^- availability. Compared with the obtained variation for NO_3^- reactions, permeable sediments acted as a sink of soluble reactive P in all treatments, regardless of salinity and NO_3^- input concentrations, indicating a possibility of P-deficiency for coastal water from the intensive cycling in permeable sediments. Furthermore, the net production of dissolved organic carbon (DOC) in all treatments was positively correlated with the measured NO_3^- reaction rates, indicating that the DOC supply may not be the key factor for NO_3^- removal rates due to the consumption by intensive aerobic respiration. Considering the intensive production of recalcitrant carbon solutes, the active denitrification was assumed to be supported by sedimentary organic matter.

Key words: NO_3^- production and removal, flow-through reactors, salinity, stable isotopes, permeable sediments

Citation: Jiang Shan, Kavanagh Mark, Severino Pino Ibánhez Juan, Rocha Carlos. 2021. Denitrification-nitrification process in permeable coastal sediments: An investigation on the effect of salinity and nitrate availability using flow-through reactors. Acta Oceanologica Sinica, 40(9): 1–12, doi: 10.1007/s13131-021-1811-5

1 Introduction

Nitrate (NO_3^-) is one of the most biogeochemically active components in the global nitrogen (N) inventory. Currently, NO_3^- storage in the biosphere is estimated to be 6.5×10^5 Tg and continues to increase due to the active anthropogenic introduction of bioactive N into the biosphere (Kuypers et al., 2018). In terrestrial ecosystems, coupled with precipitation, excess NO_3^- leaches into groundwater or surface rivers and eventually ends up in the coastal zone (Galloway et al., 2014). Apart from biological uptake in transit, coastal sediments are frequently reported as the major sink for this anthropogenic NO_3^- arriving at the littoral zone (Huettel et al., 2014).

Cohesive sediments along coastal belts are composed by a large proportion of fine particles with a capacity to accumulate organic matter, which benefits carbon food source dependent reactions (Song et al., 2013; Jiang et al., 2017a). In comparison, coastal permeable sediments are an assemblage of silicate/carbonate particles with limited organic matter storage potential (Rocha, 2008; Ibánhez and Rocha, 2014; Jiang et al., 2020). This leads to the frequent underestimation of the importance of per-

Foundation item: The National Natural Science Foundation of China under contract Nos 41706081 and 41530960; the Scientific Research Foundation of SKLEC under contract No. 2017RCDW04; the Portuguese Foundation for Science and Technology (FCT), the EU (FEDER) and the Portuguese Government through project NITROLINKS—Nitrogen loading into the Ria Formosa through Coastal Groundwater Discharge (CGD)—Pathways, turnover and LINKS between land and sea in the Coastal Zone under contract No. PTDC/MAR/70247/2006.

*Corresponding author, E-mail: sjiang@sklec.ecnu.edu.cn

meable sediments in the biogeochemical recycling of elements in the coastal zone (Rocha, 2008; Huettel et al., 2014). In coastal sediments, biogeochemical reactivity is fundamentally controlled by reactant availability, and therefore loading pathways and rates (Santos et al., 2012; Huettel et al., 2014; Ibánhez and Rocha, 2017). In cohesive sediments, apart from biological disturbance caused by infauna, diffusion is the major transport pathway of solutes between the sediment and the overlying water (Boudreau et al., 2001). In contrast, large rates of advection and dispersion are observed in permeable sediments (e.g., Huettel and Rusch, 2000). Solute transport in permeable sediments driven by advection and dispersion can be orders of magnitude higher than that caused by diffusion alone (Rocha et al., 2009, Ibánhez et al., 2011; Huettel et al., 2014). Importantly, microbial population densities on the surface of sandy particles can reach the magnitude of 10^9 cells/cm^3 (Böer et al., 2009), which is comparable to observations made in muddy sediments. Thus, a growing body of research is adding substantial evidence to the paradigm that classifies permeable sediments as a 'fast lane' for benthic biogeochemical reactions (Rocha, 2008; Gihring et al., 2009; Marchant et al., 2016; Jiang et al., 2020), including reports of high process-specific rates for NO_3^- turnover, such as denitrification, nitrification or dissimilatory nitrate reduction to ammonium (DNRA) (Santoro, 2010; Ibánhez and Rocha, 2017).

Although the importance of permeable sediments in global benthic biogeochemistry has been gradually accepted by the scientific community, there still exists a lack of in-depth understanding of the environmental drivers of biogeochemical reaction rates in permeable sediments. As aforementioned, benthic reactions are markedly modulated by environmental factors such as temperature, salinity and reactant concentrations (Santos et al., 2012; Ibánhez and Rocha, 2016, 2017). In coastal zones, these, especially salinity and reactant levels are highly variable and can be influenced by both natural processes and anthropogenic activities. An example of this is the mixing between freshwater (e.g., river water or groundwater) and seawater which modulates the salinity of coastal systems, observed in estuaries or subterranean estuaries. The loading of fresh water can also introduce terrestrial NO_3^-. In addition, discharge of sewage or runoff of fertilizers is known to enhance NO_3^- availability in coastal zones (Jiang et al., 2021). Accordingly, NO_3^- reaction rates in permeable sediments are likely to be highly variable. This leads to an uncertainty in the fate of land-borne NO_3^- and prediction of stochiometric balance between N and P in coastal waters. Currently, the knowledge about the influence of salinity and NO_3^- levels on the N turnover in permeable sediments is limited. In contrast, the environmental drivers of NO_3^- reactivity have been intensively studied in cohesive sediments and tight correlations have been observed between temperature/salinity and denitrification (Nowicki, 1994), or temperature/pH/salinity and nitrification (Jones and Hood, 1980) and redox potential and DNRA (Burgin and Hamilton, 2007). Given the capability of permeable sediments to modulate solute concentrations in coastal and shelf waters and their widespread in continental shelves (>60% coverage, Boudreau et al., 2001), the variation in NO_3^- turnover in permeable sediments caused by environmental changes may fundamentally influence NO_3^- concentration in the overlying water, potentially affecting both the ecological and the environmental status in coastal environments.

In this study, flow-through reactors (FTRs), an effective tool with many applications to simulate solute transport and reactions in permeable sediments under the 1-D advection condition (Laverman et al., 2007; Rao et al., 2007; Ibánhez and Rocha, 2014, 2016, 2017), were applied to investigate NO_3^- cycling in permeable sediments. They allow experiments to simulate advective transport that characterizes these benthic systems under controlled conditions, which permits the isolation of the effects of individual driver variability over benthic reactivity. In the present study, the permeable sediment in Dublin Bay was collected for the simulation. Dublin Bay is located at the eastern boundary of the Dublin City, Ireland (53°20′ N, 6°10′ W), facing the Irish Sea. Dublin Bay hosts several harbors for international trading with the European Union and the North America (Brooks et al., 2016). In addition, Dublin Bay is a key nursery area for fish species harvested in the Irish Sea (Brooks et al., 2016). Several surface loadings (stream and river) drain into Dublin Bay with a total rate of 2.3×10^6 m^3/d (Brooks et al., 2016). Together with tides, the outflow of the River Liffey (the main surface loading, O'Higgins and Wilson, 2005) and streams as well as the occurrence of coastal groundwater discharge (Wilson et al., 2016) leads to a patchy salinity variation within the bay. The primary research aim was to explore permeable sediments subject to variable salinity and NO_3^- input conditions, which can be identified as mimicking estuarine mixing. In addition, the microbial explanation (based on 16S rDNA analysis) for the variability of NO_3^- reaction intensity was also explored. Furthermore, the carbon source for NO_3^- reactions and the relationship between soluble reactive phosphorus (SRP) reaction and NO_3^- turnover were also investigated to reach a full view of nutrient-carbon integration in permeable sediments.

2 Materials and methods

2.1 *Sampling site and sediment characterization*

Permeable sediments were collected at the edge of the shoreline in a city park during ebbing tide in June 2016. Sediments were collected below the mean water level, and the surface layer (0–2 cm) samples were discarded due to the accumulation of algal debris. The gathered sediment was rapidly transferred to the laboratory (4 h after collection). The salinity of the overlying water was 34 at high tide and decreased to 31.5 at low tide in June, indicating a salinity variation caused by terrestrial water injection (river water or terrestrial groundwater) on the sampled sediments. Bay water temperature near the site was approximate 18°C. The grain size of the collected sediment was determined using a Beckman Coulter laser particle size analyzer. Average grain size was 0.32 mm and the proportion of clay and silt (<0.063 mm) in the sediment was low (ca. 5% in total sediment particles). Sediment porosity was approximately 0.32, determined according to the approach described in Ibánhez and Rocha (2016). Sediment organic carbon content by mass was 0.14%, quantified with the acid fumigation method of Harris et al. (2001). Total nitrogen in the sediment was 0.008% determined on a Vario EL® Cube elemental analyzer. Inorganic P in the sediment was 0.01% determined by an acid extraction method (1 mol/L HCl solution for 24 h; Aspila et al., 1976).

2.2 *FTR experiments*

The permeable sediment used in the FTR experiments was thoroughly mixed and placed into reactor cells (10 cm length, 6.6 cm diameter). Compared with the intact sediment columns, repacked sediments are homogeneous, decreasing the build-up of preferential flow during the experiments and eliminating differences in the test sediment among treatment groups (Santos et al., 2012). In addition, the FTR cells used two collimator caps and GF/F membrane filters on both sides of the sediment to remove

the possibility of particle interference and facilitate the dispersion of the circulating solution in the cells (Fig. 1). After assemblage, the reactor cells were wrapped with aluminum foil to avoid light exposure and transferred to a temperature-controlled incubator (20°C) to eliminate the influence of temperature variations on observed N reactions (Rocha, 1998, 2000) and simulate the benthic N turnover in summer in Ireland (Rocha et al., 2015).

The circulating solutions used in the FTR experiments were made with mixtures of oligotrophic marine water (salinity, 36) and river water (salinity, 0), collected from the Coliemore Harbor (53.274 8°N, 6.093 9°W) and the Phoenix Park in Dublin (53.355 8°N, 6.318 7°W), respectively. Before the experiments, the mixed solutions were aerated for 2 h to saturate dissolved oxygen (DO). To explore the effects of salinity and input NO_3^- concentration on consumption/production rates in the sediments, three treatments were employed in the experiments. The first treatment corresponds to the mixture of natural river water and marine water, and this was identified as the control. The NO_3^- concentrations in both river water and marine water were low (approximately 12 μmol/L and 2.3 μmol/L). After mixing, the final salinities of the reaction solutions were 0, 10, 15, 20, 30 and 36 (6 runs in the treatment). In the second treatment, river water was spiked with NO_3^- to a final concentration of approximately 100 μmol/L, while the seawater remained unchanged. This intends to simulate the dispersion of NO_3^- enriched freshwater along a salinity gradient in coastal zones. For the third treatment, both river water and seawater were spiked with NO_3^- to a final concentration of 100 μmol/L, eliminating the effect of mixing of fresh and marine waters over NO_3^- concentration, and therefore testing for the effect of changing salinity alone. The mixing proportions between river water and seawater in the second and third treatments were identical to the first treatment. In total, three treatments with 18 runs were included in the present study. Each run was performed in triplicate. Prior to mixing, both "endmember" water samples were filtered through GF/F filters (Whatman®; average pore size, 0.7 μm) to remove suspended particles. The flow rate of porewater in the reactor cells was 1.5 mL/min, similar to the advection rate in permeable beaches (Rocha et al., 2009; Ibánhez et al., 2011), which guaranteed the long reaction time for solutes with sediment particle surface (Jiang et al., 2018a). The input solution was pumped from the bottom to the top to simulate the 1-D advection transport in benthic environments (Fig. 1). Prior to each experimental run, the input solution was pumped through the sediment overnight (ca. 12 h) at the working porewater velocity for acclimatization. Subsequently, the run started and water samples were collected at both the input solution and the output stream (Fig. 1) every 60 min (similar to the porewater residence time in the reactor cells) for 3 h (3 collections in total). In parallel, DO content at both input and output solution was determined with an OxiCal® probe under the salinity calibration mode. Water samples for the determination of dissolved organic carbon (DOC) were stored in amber glass vials at 4°C after acidification to pH<2 using 2 mol/L HCl. Samples for fluorescent dissolved organic matter (FDOM) were stored in glass vials at –20°C. Water samples for the concentration of dissolved inorganic nitrogen (DIN) species, including NO_3^-, nitrite (NO_2^-), and ammonium (NH_4^+), as well as soluble reactive phosphorus (SRP) were stored in vacutainers at 4°C with a preservation period of less than one week (Jiang et al., 2017b). Samples for δ^{15}N-NO_3^- were stored in vacutainers at –20°C. The initial concentrations of DO, DOC, NO_3^-, NH_4^+, NO_2^- and SRP at each run are outlined in Supplementary Table S1.

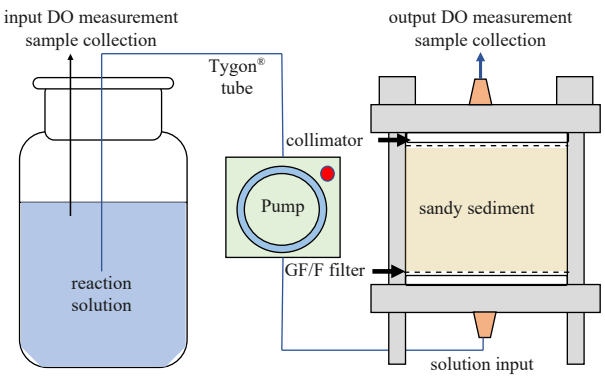

Fig. 1. Sketch of the FTR experimental setup. The sketch includes two DO measurements and sample collection points (from the input solution reservoir and the output stream). The figure is based on Jiang et al. (2018a).

2.3 *Analytical methods*

DOC was determined on a Vario TOC Cube elemental analyzer after purging with carbon-free gas (CO_2 and VOC free air; 10 min per sample). The detection limit for DOC was approximately 14 μmol/L based on the determination blanks. The method precision was ca. 6%. FDOM was measured on a Cary Varian Eclipse® spectrofluorometer via 3-D excitation-emission-matrix spectral scanning (Ibánhez and Rocha, 2014) and subsequently processed with the DOM Fluor Toolbox in MATLAB (Stedmon and Bro, 2008). Water from a Millipore purification gradient system was used as blank. The signal from the daily blanks was subtracted from the sample spectra to remove Raman scatter peaks (Stedmon and Bro, 2008). Fluorescence intensities for each sample were divided by the integrated area of Raman peaks from the blank (Lawaetz and Stedmon, 2009). Consequently, results were expressed in Raman units (R.U.). Parallel Factor Analysis (PARAFAC) was used to decompose the fluorescence signal and to obtain the main fluorophores present in our dataset (Stedmon and Bro, 2008). The results of the PARAFAC modelling were validated by split-half analysis provided in the tool box.

The concentration of NO_3^-, NO_2^-, NH_4^+ and SRP in all water samples were determined using a Lachat Quickchem-8 500 Flow Injection Analysis system according to standard colorimetric methods (Hansen and Koroleff, 1999). The equipment detection limit for all these solutes was below 0.3 μmol/L and the method precision was higher than 4%. δ^{15}N-NO_3^- was determined using the bacterial reduction method (*Pseudomonas aureofaciens*; Sigman et al., 2001) after removal of NO_2^- (Weigand et al., 2016). N_2O produced from the NO_3^- reduction vials were concentrated in a Thermo-Fisher Precon system (Thermo Fisher, USA) via a liquid nitrogen loop with subsequent flow-through Finngan chromatographic loops and finally into a Thermo-Fisher Delta V Advantage isotope system (Jin et al., 2020). The method precision was ca. 0.2‰ based on the long-run. Calibration was made using commercial standards (USGS 32, 34, 35; IAEA-NO_3^-).

Sediment microbiota of the mixed sediment preserved at –20°C was quantified as the 16S rRNA gene fragments to determine the microbial community structure. Briefly, DNA from approximately 0.3 g thawed sediment was extracted and V3-V4 regions of 16S rRNA genes were then amplified after 35 PCR cycles. After library construction using KAPA Hyper Prep Kit (Roche), the obtained library was paired-end sequenced on an Illumina Miseq system (Jiang et al., 2020). The potential functional pro-

files of sediment microbiota were predicted in R environment using an open-source package that identifies the functional capabilities of microbial communities based on 16S rRNA marker gene profiles (AßHauer et al., 2015; Wang et al., 2020).

2.4 *Data statistics and analysis*

The mean concentration of solute in each treatment was the average from three reactors. The reaction rate for each solute was calculated with the input-output concentration difference from the individual reactor according to Ibánhez and Rocha (2014) and the mean rate was the average of the three reactors. Accordingly, the statistical errors from the concentration variation between reactors could not propagate to the reaction rate calculation and reduce the standard deviation. Positive reaction rates indicate the production of a specific solute and negative reaction rates represent a net consumption. To identify the effects of different salinity and input NO_3^- concentration on reaction rates, the data were analyzed in Minitab 18 by one-way ANOVA (tested factor, such as salinity or NO_3^- input concentration) after checking for normality and homogeneity of variance at a 95% significance level.

3 Results

3.1 *Sediment microbiota*

The operational taxonomic units in the sediment were 1 705. These operational taxonomic units were identified as more than 10 phyla with the dominant phylum as Protobacteria (Table 1). Important opportunity phyla included Actinobacteria, Bacteroidetes and Firmicutes. Among these phyla, the majority was identified as heterotrophic and actively involved in the nitrogen, oxidative and sulfur metabolism (Supplementary Fig. S1). At the class-level, the dominant species was Alpha-proteobacteria (Table 1). For the microbiota involved in the NO_3^- biogeochemical processing, the dominant nitrifier in the sediment was *Nitrosomonas* and *Nitrospira*, while potential denitrifiers were mainly identified as *Bacillus*, *Lactobacillus* and *Paracoccus* (Table 1).

3.2 *DO and DOC*

In all the experiments, DO concentrations at the input endmember were near saturation. After passing through the reactor cells, DO concentrations markedly decreased (Figs 2a–c). In the control (i.e., with waters not amended with NO_3^-), DO concentrations in the outflow varied between 257 and 194 μmol/L. Accordingly, DO consumption rates ranged between 9.2 nmol/cm^3 and 15.6 nmol/cm^3 sediment per hour with the highest value recorded at intermediate salinity (20). In the remaining treatments, the addition of NO_3^- did not significantly influence the DO concentration in the outflow. Accordingly, DO consumption rates among the treatments showed similar distribution along the used salinity range (p>0.05).

In the control, DOC concentration in the input solutions from

Table 1. Relative frequency of the top 5 phyla and classes in the sediment microbiota, and at the genus level, five key species were outlined with regard to N production (nitrification) and removal (denitrification) and their frequency was shown

Phylum	Frequency/%	Class	Frequency/%	Genus	Frequency/%
Proteobacteria	41.8	Alpha-proteobacteria	16.6	*Nitrosomonas*	0.02
Actinobacteria	13.6	Gamma-proteobacteria	14.5	*Nitrospira*	0.04
Firmicutes	9.9	Actinobacteria	11.0	*Bacillus*	0.05
Bacteroidetes	5.9	Betaproteobacteria	6.2	*Lactobacillus*	0.01
Acidobacteria	5.1	Bacilli	1.2	*Paracoccus*	0.01

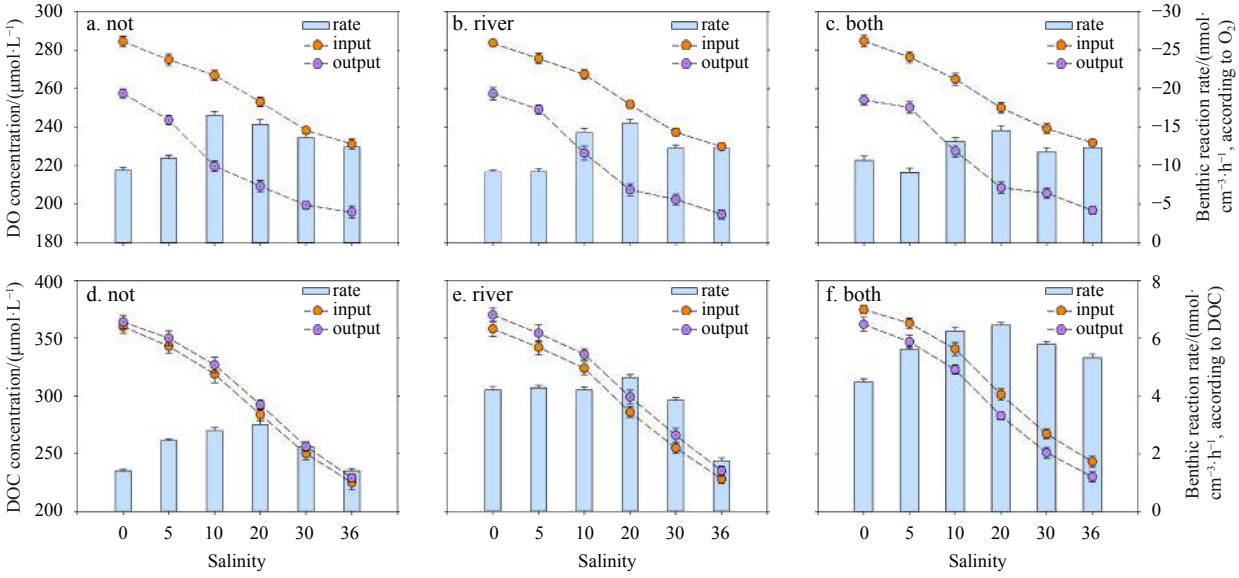

Fig. 2. Concentrations of DO and DOC at both input reservoir and output stream (dot plot) and benthic reaction rates (bar chart) in the three scenarios simulated: not amended, natural river and seawater (a and d); river water amended with NO_3^- (b and e) and both river and seawater amended with NO_3^- (c and f). Positive rate indicates production while negative rate indicates consumption. "Not" indicates the control treatment; "river" indicates the river spiked treatment; "both" indicates the treatment where both river water and seawater received NO_3^- amendment. Data represent mean±standard deviation.

360 μmol/L (river water) to 225 μmol/L (seawater). After flowing through the reactor columns, DOC concentrations increased in all salinity treatments (Fig. 2d), indicating that permeable sediments acted as a source of DOC. The highest production rate was 3.0 nmol/(cm^3·h) at a salinity of 20. When additional NO_3^- was introduced into the system, DOC concentrations at the output stream were also higher than the values obtained at the input solution (Figs 2e and f). Compared with the control group, the DOC production rates from the two NO_3^- spiked treatments were significantly higher (p<0.05).

3.3 NO_3^- and δ^{15}N-NO_3^-

At the output of the control group, NO_3^- concentrations increased, leading to an active production trend (Fig. 3a). When river water was spiked with NO_3^-, the sediments (salinity 0 to 30) shifted to a net sink for NO_3^- with the most active NO_3^- removal occurring at a salinity of 10 (Fig. 3b). In addition, the active NO_3^- removal further enhanced the sediment DOC production capability (Fig. 4a). When maintaining high and similar NO_3^- concentration levels at all the salinities used (3rd treatment), NO_3^- reduction rates at high salinity markedly increased (Fig. 3c), producing a linear correlation between NO_3^- removal rates and salinity (Fig. 4b). Due to the identical NO_3^- input concentrations in the 3rd treatment, no clear pattern was found between NO_3^- reaction rates and NO_3^- concentrations (Fig. 4c), while two parabolic lines were outlined in the 2nd treatment, suggesting the impacts from NO_3^- availability on its benthic removal. Coupled with NO_3^- reaction dynamics, δ^{15}N-NO_3^- co-varied, NO_3^- production in the control group triggered decreases in δ^{15}N-NO_3^- (Fig. 3d), while the occurrence of NO_3^- consumption led to an increase in δ^{15}N-NO_3^- in all cases (Figs 3e and f). NO_3^- reaction rates, including production and consumption, showed a linear correlation with the $\Delta\delta^{15}$N-NO_3^- (difference in δ^{15}N-NO_3^- between output and input) as outlined in Fig. 4d.

3.4 NH_4^+ and NO_2^-

In the control, after passing through the sediments, NH_4^+ concentrations significantly increased (p<0.05) with higher production rates in the 10–30 salinity range (Fig. 5a). When exogenous NO_3^- was added, the sediments continued to act as a source of NH_4^+. However, reaction rates dropped (p<0.05), especially in the intermediate salinity runs (Figs 5b and c). For NO_2^- in the control, the sediment was an active producer and concentrations peaked at salinities of 10 and 20 (Fig. 5d). In contrast, after NO_3^- addition, NO_2^- cycling in the sediments changed. Both NO_2^- production and removal were observed, randomly distributed along the salinity gradient. Moreover, the magnitude of reaction rates shrank (Figs 5e and f).

3.5 SRP

SRP concentrations in the input endmembers were lower than 1.2 μmol/L in the control group (Fig. 5g). SRP concentrations at the outflow water dropped, resulting in a net SRP consumption. This SRP consumption tended to remain similar among the different salinity treatments. Moreover, the addition of NO_3^- did not significantly influence SRP removal rates (Figs 5h and i).

3.6 FDOM

Four FDOM components were identified via PARAFAC modeling of our FDOM dataset. The characteristic excitation and emission wavelength of each fluorophore are outlined in Table 2. The first FDOM fluorophore is similar to the spectra of pure tyrosine. It corresponds to the so-called Peak B in the Coble nomenclature (Coble, 1996) while FDOM Component 2 is similar to the spectra of pure Tryptophan and corresponds to Peak T (Coble, 1996). They both are associated to labile, low molecular weight, protein-like FDOM compounds (Stubbins et al., 2014). Their maximum fluorescence intensities (F_{max}) varied between approximately 0.08 to 0.16 R.U. in the input solutions used in all treatments. The ratios between input and output F_{max} were frequently higher than 1 (i.e., net production) along the salinity gradient employed for both protein-like FDOM components, particularly pronounced in the case of the intermediate salinity runs (Figs 6a

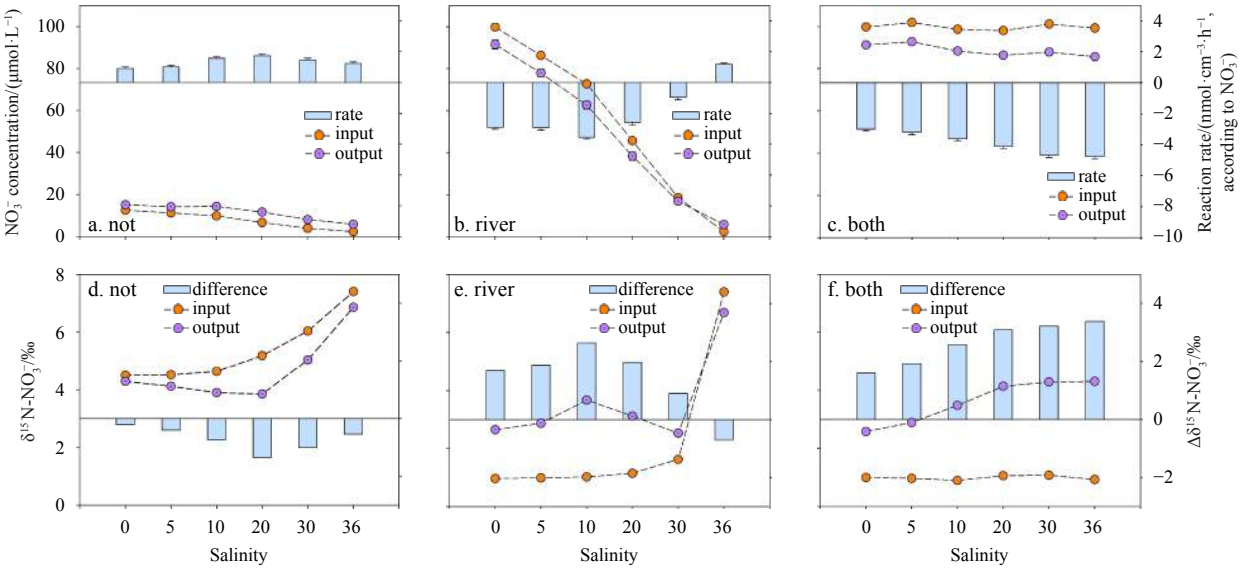

Fig. 3. NO_3^- concentrations at both input reservoir and output stream (dot plot), as well as reaction rates (bar chart) under unamended conditions (a), NO_3^- amended river water (b) and both river and seawater amended with NO_3^- (c). Figures in bottom panel present the δ^{15}N-NO_3^- and the differences in the isotopic composition of nitrate between the input reservoir and the output stream ($\Delta\delta^{15}$N-NO_3^-) under control conditions (d), NO_3^- amended river water (e) and both river and seawater amended with NO_3^- (f).

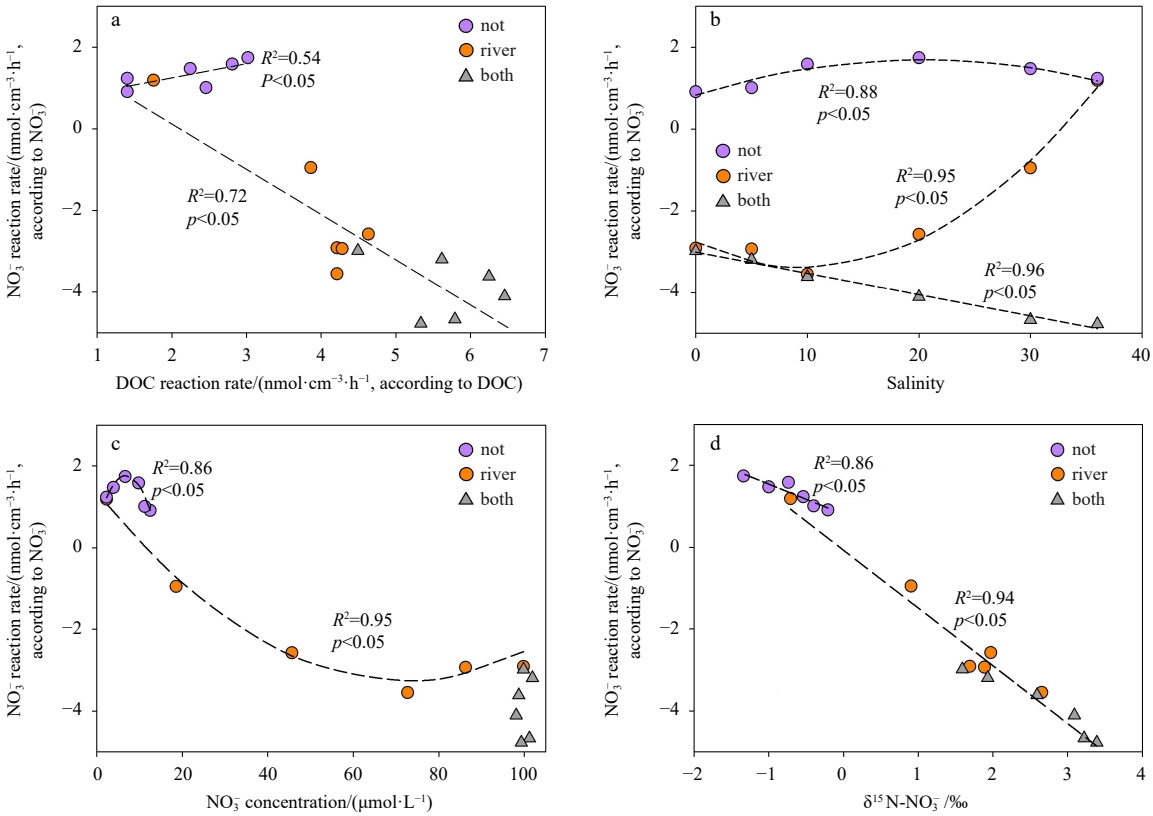

Fig. 4. Correlations between NO_3^- reaction rates with DOC reaction rates (a), salinity (b), NO_3^- concentration (c), and δ^{15}N-NO_3^- (d) under unamended (not), river water amended (river) and both river water and seawater amended (both) conditions.

and b). In the experiments amended with NO_3^-, the input-output balance was also frequently higher than 1, especially in the salinity range of 10 to 30.

The other two FDOM components identified through PARAFAC modelling of our dataset correspond to two types of recalcitrant FDOM, terrestrial humic (Peak C) and microbial humic-like FDOM fluorophores (Peak M; Coble, 1996). These corresponds to high molecular weight, complex humic and fulvic substances of low degradability (Stubbins et al., 2014). In our experiment, both humic-like components showed that the sediment acted always as a source of these compounds to the circulating porewater (Figs 6c and d). Under low NO_3^- concentrations in the circulating porewater (control treatment), maximum production of these FDOM components was verified at intermediate salinities, similar to the two protein-like FDOM components. Nevertheless, when high with NO_3^- concentrations were presented (i.e., at low salinities in the 2nd treatment and in the entire 3rd treatment), an enhancement in the production of the two humic-like FDOM components is observed (Figs 6c and d).

4 Discussion

4.1 *Reaction rates obtained with FTRs in permeable sediment studies*

FTRs are powerful tools to investigate biogeochemical reactions in permeable sediments under the 1-D advection condition. Still, porewater transport processes in FTRs are not directly comparable with fluid circulation in "real world" conditions. Specifically, in natural environments, solute transport between permeable sediments and overlying water is largely dependent on advection resulting from the pressure gradient caused by waves, current interaction with topography, tide or piezometric head among other process (Rocha, 2008). The advection rate thus is variable in time but also spatially, as the interfacial flow direction at any point is controlled by the local permeability tensor (Rocha et al., 2005). Due to the tight coupling among reaction rates and advective transport in permeable sediments (Rocha, 2008; Ibánhez et al., 2011; Huettel et al., 2014), direct extrapolation of reaction kinetics and relationships between biogeochemical transformations and environmental variables obtained with FTR experiments requires a "double-check" via a data comparison.

DO, NO_3^- and SRP reaction rates obtained in this study are comparable to others previously published FTR studies or simulation results. In the current research, DO consumption rates ranged from 92 nmol/(cm^2·h) to 156 nmol/(cm^2·h) for the entire sediment column (10 cm sediment column). These values are in the range of those obtained in different marine permeable sediments such as those found by Ibánhez and Rocha (2016) in the Ria Formosa Lagoon using the FTR technique (56 nmol/(cm^2·h) to 168 nmol/(cm^2·h), according to O_2) and Rao et al. (2007) in sediments from the South Atlantic Bight using a series of 15.8 cm length of FTRs (86.9 nmol/(cm^2·h) to 240 nmol/(cm^2·h), according to O_2). These are also comparable to the benthic chamber incubations in the German Bight using (120 nmol/(cm^2·h) to 160 nmol/(cm^2·h), according to O_2; Janssen et al., 2005).

Present results for NO_3^- production rates (0.4 nmol/(cm^2·h) to 21 nmol/(cm^2·h) for the 10 cm sediment column) are also comparable to a series of incubation experiments targeting permeable sediments, such as nitrification rate estimates in the Ria Formosa Lagoon (7.0 nmol/(cm^2·h) to 10.4 nmol/(cm^2·h); Ibánhez and Rocha, 2017) and the German Bight (2.2 nmol/(cm^2·h)

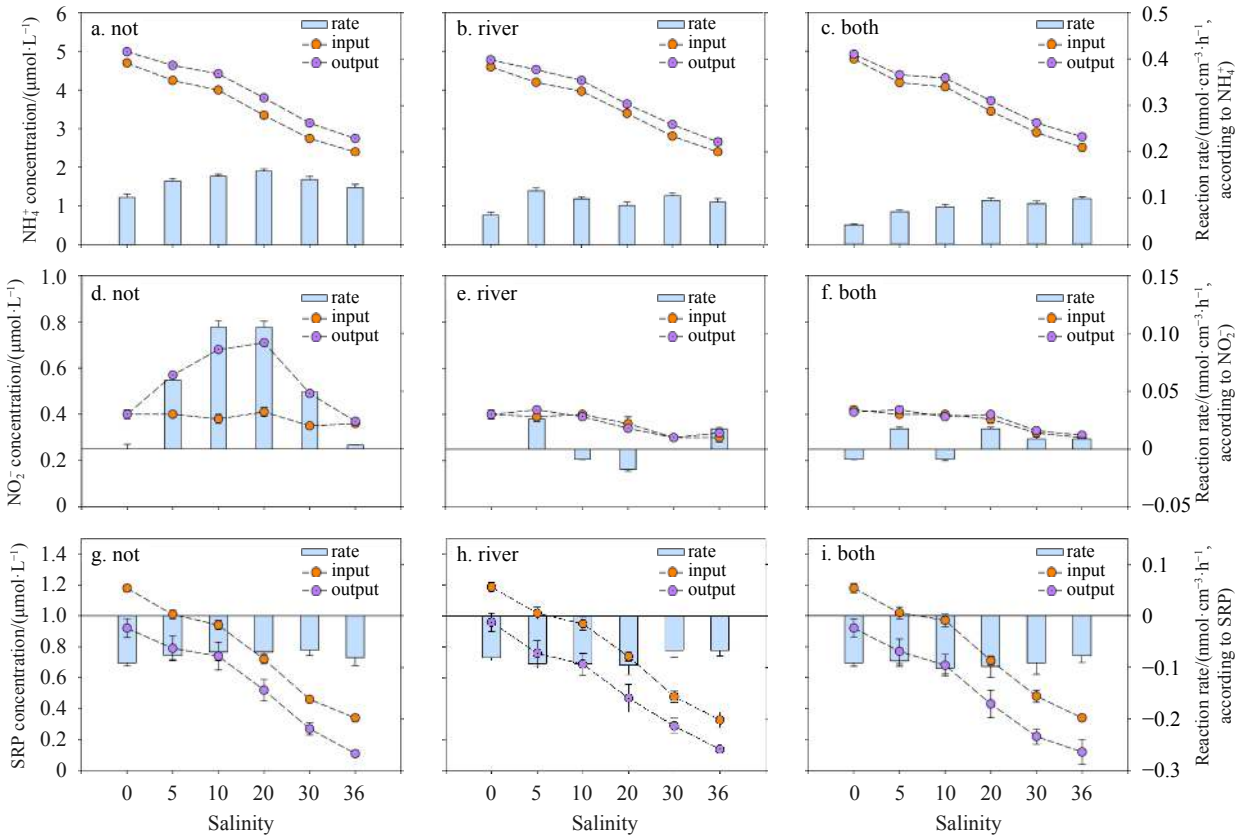

Fig. 5. Concentrations of NH_4^+ and NO_2^- at both input reservoir and output stream (dot plot), as well as reaction rates (bar chart) under unamended conditions (a and d), NO_3^- amended river water (b and e) and both river and seawater amended with NO_3^- (c and f). Concentrations of SRP at both input and output members (dot plot) and its reaction rates (bar chart) under unamended condition (g), spiked river (h) and both river and seawater amended with NO_3^- (i). Data represent mean±standard deviation.

Table 2. Excitation and emission peaks obtained using PARAFFAC for each FDOM component in the present study and relative concentrations of each solute for the input water in river water and seawater (the identification of these FDOM solutes was completed via comparison with a series of publications listed in the table)

Solute	Excitation peak/nm	Emission peak/nm	Relative concentration/R.U.	
			River water	Sea water
Tyrosine	235	320	0.16±0.02	0.09±0.01
Tryptophan	235	350	0.19±0.01	0.08±0.01
Terrestrial humic	255	460	0.24±0.02	0.05±0.01
Microbial humic	230	430	0.09±0.01	0.04±0.01

to 9.4 nmol/(cm²·h); Marchant et al., 2016). In terms of the NO_3^- reduction rates, our results (9.8 nmol/(cm²·h) to 48 nmol/(cm²·h)) are comparable to those obtained by Jiang et al. (2018a) (7.0 nmol/(cm²·h) to 68 nmol/(cm²·h)) who applied similar input NO_3^- concentrations in FTR experiments run with Ria Formosa sediments. The rapid removal of SRP in the test sediments also agrees well with several publications on SRP sorption dynamics in sandy coastal sediments (e.g., Leote et al., 2013; Yang et al., 2018).

4.2 *Benthic NO_3^- reactivity along the salinity gradient*

NO_3^- production and reduction showed significantly distinct rates among the three treatments tested in our experiments (control, river water amended with NO_3^- and all amended with NO_3^-). The net NO_3^- production observed in the control treatment suggests the dominance of nitrification over NO_3^- reduction, likely due to the low levels of NO_3^- and DO saturation imposed in the input solutions. This is generally observed in pristine (NO_3^- unpolluted) estuaries in remote regions (Seitzinger, 1987; Jiang et al., 2019). The intensity of net NO_3^- production changed along the salinity gradient imposed, with a clear accumulation of both NO_3^- and NO_3^- at intermediate salinities (~20, Figs 3a and 5d). Coupled with enhanced NO_3^- production at intermediate salinities, $\delta^{15}N$-NO_3^- decreased, indicating the occurrence of enhanced nitrification (Marchant et al., 2016). Similar enhanced NO_3^- production at intermediate salinities were found by Zhou et al. (2017) and Magalhães et al. (2005) in benthic habitats.

In the control, NH_4^+, i.e., the substrate for nitrification, did not show consumption rates equivalent to the net NO_3^- production observed. Hence, the studied permeable sediments acted as a source of NH_4^+. In permeable sediments, several sources might be contributors to the porewater NH_4^+ pool. N fixation, mediated by benthic microbiota, including a wide range of Alpha-proteobacteria (Dekas et al., 2018), should be considered as an important contributor (outlined in Fig. 7). Notably, carbon supply has been frequently found to be a pivotal factor for fixation activity

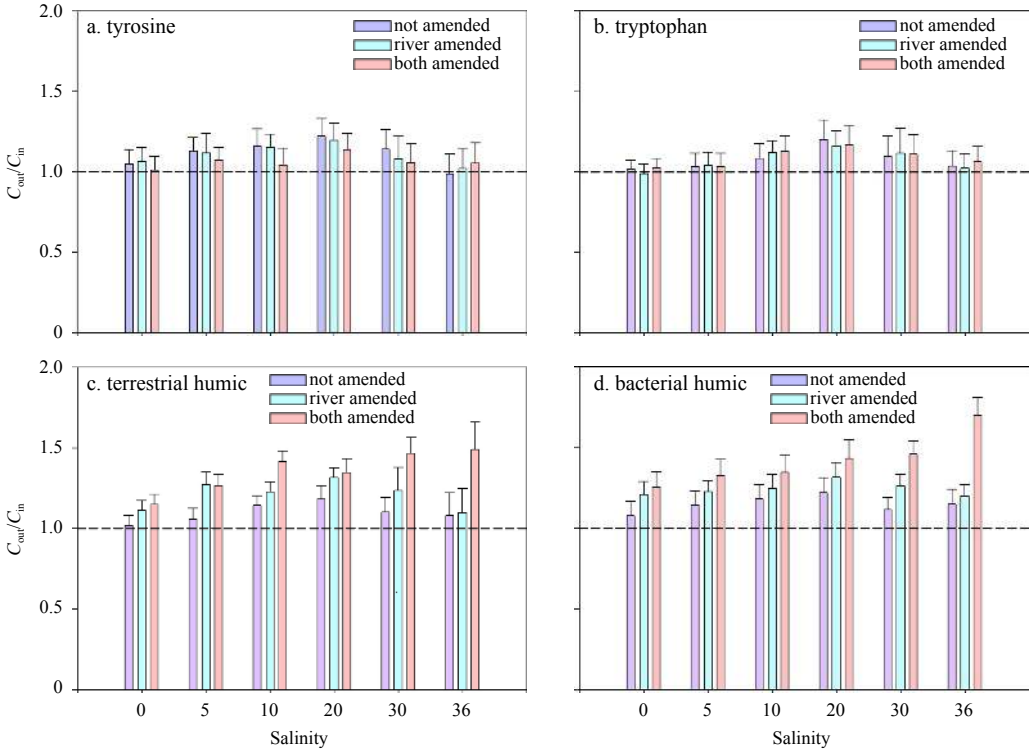

Fig. 6. Comparison on the relative intensities of the four FDOM components identified through PARAFAC analysis between the input reservoir and the output stream under the three experimental scenarios: a. tyrosine-like FDOM component; b. tryptophan-like FDOM component; c. terrestrial humic-like FDOM; d. marine bacterial humic-like FDOM. *C* indicates concentration, the dash line indicates the ratio of 1 (input = output).

(Changjiang River Estuary, Hou et al., 2018; Hydrate Ridge, Dekas et al., 2018). In the present study, the sediment organic matter was limited due to the nature of the "sands" and the input solution was oligotrophic, indicating that N fixation via Alphaproteobacteria was depressed. NH_4^+ desorption from the sediments due to changes in the partition coefficient induced by varying salinity (Ibánhez and Rocha, 2017) also impacts porewater NH_4^+ levels, while this effect might be minimized in the incubation period, due to 12 h FTR stabilization prior to the sample collection. Accordingly, the main source of NH_4^+ feeding nitrification should be that produced through mineralization and ammonification. Considering that DOC and labile FDOM were not consumed in the different treatments, sedimentary organic matter (SOM) seemed to be the main carbon source to support the intensive oxidative metabolism (Supplementary Fig. S1), especially aerobic respiration. This agreed with the observation of Jiang et al. (2018a) and Ibánhez and Rocha (2014), who found that, despite low SOM levels in permeable sediments of Ria Formosa, these acted as net sources of DOC. During SOM decomposition via heterotrophic processes, organic N is mineralized into inorganic fractions and these products can be nitrified (outlined in Fig. 7). Such reaction chain leads to the coupling of SOM aerobic mineralization and nitrification in benthic environments, as outlined by the DOC production and nitrification rate in Fig. 4a. The decrease of $\delta^{15}N\text{-}NO_3^-$ reinforces the occurrence of active nitrification in the 1st treatment. According to the intensive requirement (first-order kinetics) on the substrate availability in benthic nitrifiers (Ibánhez and Rocha, 2017), it is not surprising to find the pattern that high reaction rate of nitrification at intermediate salinities in the control treatment is obtained. This reaction peak is in line with results from experiments run by Chambers et al. (2013), who also show nitrification is stimulated at intermediate salinities. Moreover, salinity increase leads to a reduction of NH_4^+ adsorption potentials of estuarine sediments (Weston et al., 2010), indicating that NH_4^+ produced from mineralization or NH_4^+ adsorbed on sand particles could be more rapidly available for nitrification.

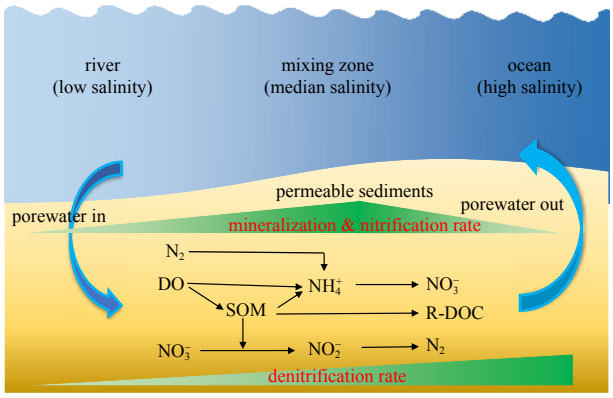

Fig. 7. Sketch for the DIN removal and addition along the salinity gradient coupled with river-sea mixing. It highlights the potential reaction pathways and reaction intensity peaks. SOM, sedimentary organic matter.

The variability of nitrification rates under different salinities may also result from the composition of the nitrifier microbial community. Two types of nitrifiers, ammonia-oxidizing *Archaea* (AOA) and ammonia-oxidizing *Bacteria* (AOB) have been identified in coastal sediments (Bernhard and Bollmann, 2010). In the

collected sediment, AOB was the dominant nitrifier in sediments with high-abundance *Nitrosomonas* and *Nitrospira* (Table 1). Salinity preferences have widely been identified in both nitrifiers. For instance, *Nitrospira* showed a great abundance at salinity of 3.4 along Chinese tidal flat wetlands (Sun et al., 2020). Jones and Hood (1980) isolated *Nitrosomonas* strains from the salt marsh at Lac des Allemands, USA that showed an activity peak at salinity 6 to 10. Wang and Gu (2014) revealed that the growth of *Nitrosomonas* strains in mangrove sediments (Mai Po Nature Reserve) was stimulated by saltwater (salinity, 20). Although there exist differences in the microbial community composition between sites, these observed salinity-preference patterns suggest that nitrification rates in coastal sediments are likely to occur at increasing salinity in the mixing gradient between fresh and seawater and peak at the medium salinity (brackish environment). During the short-term incubation, the variation of microbial community in the sediment was assumed to be limited (Mariotti et al., 1981), supported by the linear correlation between δ^{15}N-NO_3^- and reaction rates (Fig. 4d). Alternatively, the salinity induced microbial activity variation is deemed to be responsible for the reaction intensity change.

When external NO_3^- was introduced into the system, the balance between NO_3^- production and removal in the studied permeable sediment markedly changed, shifting to a net sink for NO_3^-. Furthermore, compared to the control treatment, NO_2^- in the porewater sustained at low-level, indicating a rapid transformation for nitrogen oxides in the sediment. However, the production/reduction of NO_3^- in the 2nd and 3rd treatments along the salinity gradient was markedly different, suggesting overlapped influences from both salinity and NO_3^- concentration changes. With an identical NO_3^- input throughout the salinities used (3rd treatment), NO_3^- removal rates peaked and δ^{15}N-NO_3^- enrichment in the highest salinity scenario (Figs 3c and f). In the benthic environment, though the presence of Anammox, denitrification is assumed to be the major contributor of NO_3^- removal, especially in the aerobic condition (Burgin and Hamilton, 2007). In the present study, a high abundance of potential denitrifers in the sediment was observed, while microbial carriers for Anammox (e.g., *Pirellula* and *Planctomyces*) were not obtained (Table 1). Additionally, the combination of increased δ^{15}N-NO_3^- and high NO_3^- removal rates (Fig. 4d) reinforces the presence of dominant removal reaction, i.e., denitrification here, for the NO_3^- concentration decreases (Granger et al., 2008).

In previous research, positive relationships between salinity and benthic denitrification or NO_3^- reduction were observed (Laverman et al., 2007; Marks et al., 2016; Zhou et al., 2017). The denitrification process can be conducted by a wide range of bacteria. These bacteria have distinct salinity preferences (Santoro et al., 2006). The bacteria frequently observed in the marine environment, e.g. *Pseudomonas* sp. and *Marinobacter* sp. (Yoshie et al., 2004), are still functional in the freshwater environment (Yoshie et al., 2004; Miao et al., 2015), while the inverse trend might not be as likely because of the high osmotic pressure in the saline environment. In wastewater treatment reactors, *Bacillus* and *Paracoccus* were frequently observed and showed higher activity with increasing salinity (Silva et al., 2018). Moreover, *Bacillus* was frequently isolated in marine environments, such as shrimp culture ponds (Song et al., 2011). Additionally, at the time of sediment collection during the present study, the salinity of the overlying water in the sampling site was 34 (high tide) and 31.5 (low tide). Thus, it would not be surprising to observe the highest NO_3^- consumption rate in the most saline treatment when amended with NO_3^-.

In freshwater ecosystems, such as rivers and groundwater, widespread anthropogenic enrichment of NO_3^- due to the intensive application of chemical fertilizers, sewage discharge, and manure disposal is observed (Galloway et al., 2014). The mixing between freshwater and seawater in the coastal zone can produce large spatial and temporal gradients in both salinity and NO_3^- concentration. Under such circumstance, the peak of denitrification occurred in the intermediate salinity (Fig. 4b), outlined by the 2nd treatment. Given the strong reaction potential in the saline environment, the occurrence of this peak indicates the balance between NO_3^- supply and salinity. In low salinity waters, because the NO_3^- supply was sufficient (>60 μmol/L here; five times higher than the riverine NO_3^- concentration, Fig. 3b), salinity mediated bacterial activity was the dominant factor controlling NO_3^- removal rates, producing a negative correlation between NO_3^- concentration and denitrification rate (Fig. 4c). Under high salinity conditions, the dilution from a large portion of oligotrophic seawater decreases NO_3^- concentration. As a reaction strictly driven by the substrate availability, the significant requirement of NO_3^- from denitrifiers and the constraint of NO_3^- on denitrification rate has been determined via *in situ* observation (seepage face; Ibánhez et al., 2011), simulation experiments (FTRs; Jiang et al., 2018a), as well as denitrifier-inoculated reactors (Jafari et al., 2015). Moreover, in laboratory culture, nitrate reductase in *Bacillus* (potential denitrifier at our site) was also proved to be activated by high-level NO_3^- in culture solution (Schulp and Stouthamer, 1970). Accordingly, it can be deduced that sediment denitrification processes at high salinity from the 2nd treatment was constrained by NO_3^- supplies due to seawater dilution, especially compared to the highest NO_3^- consumption rate measurement when seawater was spiked with NO_3^- (3rd treatment).

In coastal zones, this trend can be a key factor in understanding the modulation of land-derived NO_3^- conducted through permeable sediments (transformation pathways outlined in Fig. 7). In oligotrophic environments, permeable sediments continuously provide NO_3^- into the overlying water via organic matter mineralization and nitrification, which can be used by primary producers. Enhanced NO_3^- loading from human activities stimulates sediment denitrification and initiates the role of "NO_3^- cleaner". This balance between these contrasting roles in benthic sediments may help the coastal system maintain primary productivity and ecological stability, acting as a "nutrient modulator" (Huettel et al., 2014). Moreover, compared to the rapid shift in the role played in the NO_3^- processing, the preferential salinity of sediment microbial community was stable in a short temporal scale (3rd treatment). It suggests that environmental stresses in coastal systems result from the coupling of intensive NO_3^- loading and fresh water discharge (triggered by weather extremes, such as floods in the upper stream driven by storms) and might exceed the NO_3^- removal capability deduced from saline environments. Consequently, a significant fraction of redundant NO_3^- might temporally escape from the benthic sediment and transfer into the food web, triggering unexpected ecological issues. This potential input-feedback loop deserves more attention from a coastal management perspective, especially in the handling of weather extremes.

4.3 *Benthic coupling among NO_3^-, SRP and organic matter processing*

Notably, in the present study, NO_3^- removal occurred in overall oxic conditions, indicating that denitrifiers rely on microniches on the surface of the sediment particles (Jiang et al.,

2018a). Coupled with NO_3^- reduction, SOM was continuously decomposed, releasing additional DOC fractions (linear regression in Fig. 4a) such as humic-FDOM solutes into the porewater when compared with the control treatment (Figs 6c and d). This observation agrees well with FTR experiments conducted with sediments from the Ria Formosa Lagoon (Ibánhez and Rocha, 2014), where the addition of NO_3^- to the circulating porewater enhanced DOC and humic-like FDOM production. In their experiments, SOM was characterized by a relatively high C:N concentration ratio, similar to that found in our sampling site (C:N=15), which together with low standing stocks of SOM explains the observed C limitation of the microbial community of Ria Formosa permeable sediments (Ibánhez and Rocha, 2014). Nevertheless, enhanced humic-like FDOM production, linked to active organic matter degradation, after NO_3^- addition to the porewater suggest that the microbial community was also N limited. Thus, as in our case, NO_3^- addition increases the capacity of the microbial community to process SOM thus favoring heterotrophic processes.

Coupled with the active metabolism functions (Supplementary Fig. S1), especially benthic mineralization and denitrification, that continuously consume SOM, release of SRP into the porewater should be observed in all treatments. In addition, increasing salinity potentially benefits the SRP desorption process because of enhanced ion exchanges on the particle surface. However, low SRP concentrations and the related net consumption are found in the outflow, regardless of salinity and DO consumption rates. Considering that primary production in the sediments was eliminated by imposing dark conditions and that oxic conditions were imposed, SRP adsorption on the sandy sediment particles due to the presence of metal oxidants, such as iron and manganese, was deemed to be responsible for the observed SRP concentration decline (Yang et al., 2018). In fact, inorganic P content in the tested sediment was higher than the concentration of sedimentary N, which was contrary to the Redfield ratio (N:P=16:1). This reinforces the strong SRP adsorption capability of coastal sediments on overlying water or porewater (Jiang et al., 2018b). In marine environments, the stoichiometric balance between N and P is a key for the phytoplankton community structure (Lin et al., 2020). Our results show that under oxic conditions, permeable sediments from the Dublin Bay may increase the N:P ratio in the outflow relative to the Redfield ratio, potentially driving the system to P-limitation. This change might induce phytoplankton community shift from the diatom-dominance to dinoflagellate-dominance due to the weak N competition capability of diatoms (Rocha et al., 2002), particularly together with the variation in water temperature (Li et al., 2011). Generally, diatoms are the most important primary supplier in the food web and directly contribute to filter feeding fish and shellfish populations. In comparison, dinoflagellates are an unfavored food source for high-level consumers due to toxin defensiveness (Verma et al., 2019). Therefore, long-term P adsorption in permeable sediments during the porewater exchange might lead to ecological pressures. In addition, when redox conditions change (aerobic to anaerobic), adsorbed P in the permeable sediments would be released into the overlying water (Jiang et al., 2018b), potentially driving the system to N limitation. Such shift between N and P limitation caused by permeable sediments could be of extreme importance for the biological structure of shallow coastal waters.

5 Conclusions

The present study focused on biogeochemical reaction rates (mainly denitrification and nitrification) in permeable sediments subject to different salinities and initial NO_3^- concentrations. At low NO_3^- availability, net NO_3^- production and decreases in δ^{15}N-NO_3^- occurred in the test sediments throughout the used salinity gradient. The peak of NO_3^- production, resulting from nitrificaiton, was found at an intermediate salinity (10), likely due to enhanced mineralization of SOM and active ammonification at this aerobic environment. When additional NO_3^- was introduced into the river water while seawater remained unchanged, permeable sediments turned into a sink for NO_3^-, mainly due to stimulated denitrification (likely carried out by *Bacillus*, *Lactobacillus* and *Paracoccus*), suggesting that denitrification in the permeable coastal sediment was constrained by NO_3^- availability. This hypothesis was testified in the 3rd treatment. Both NO_3^- consumption rates and δ^{15}N-NO_3^- at the output peaked in the most saline water when NO_3^- availability was constant along the salinity gradient. The salinity preference of local denitrifiers may be the main reason for the peak of removal. The reaction balance between NO_3^- addition and removal in permeable sediments can modulate NO_3^- concentrations in shallow coastal waters, exerting control over the biomass of primary producers. In contrast to the variable NO_3^- turnover, permeable sediments acted as a sink for SRP regardless of NO_3^- availability, likely due to adsorption under the imposed aerobic conditions. This relatively high storage of SRP within the sediment may be released if redox potential in the overlying water changes, and this factor deserves more attention from coastal managers and other stakeholders.

Acknowledgements

We gratefully acknowledged technical support during the laboratory analyses by Tara Kelly, Alexandra Oppelt and Jie Jin. We are thankful to two anonymous reviewers whose comments helped to improve an earlier version of the manuscript.

References

Aspila K I, Agemian H, Chau A S Y. 1976. A semi-automated method for the determination of inorganic, organic and total phosphate in sediments. Analyst, 101(1200): 187–197, doi: 10.1039/AN9760100187

Aßhauer K P, Wemheuer B, Daniel R, et al. 2015. Tax4Fun: predicting functional profiles from metagenomic 16S rRNA data. Bioinformatics, 31(17): 2882–2884, doi: 10.1093/bioinformatics/btv287

Bernhard A E, Bollmann A. 2010. Estuarine nitrifiers: new players, patterns and processes. Estuarine, Coastal and Shelf Science, 88(1): 1–11, doi: 10.1016/j.ecss.2010.01.023

Böer S I, Hedtkamp S I C, Van Beusekom J E E, et al. 2009. Time- and sediment depth-related variations in bacterial diversity and community structure in subtidal sands. The ISME Journal, 3(7): 780–791, doi: 10.1038/ismej.2009.29

Boudreau B P, Huettel M, Forster S, et al. 2001. Permeable marine sediments: overturning an old paradigm. Eos, Transactions American Geophysical Union, 82(11): 133–136, doi: 10.1029/EO082i011p00133-01

Brooks P R, Nairn R, Harris M, et al. 2016. Dublin Port and Dublin Bay: Reconnecting with nature and people. Regional Studies in Marine Science, 8: 234–251, doi: 10.1016/j.rsma.2016.03.007

Burgin A J, Hamilton S K. 2007. Have we overemphasized the role of denitrification in aquatic ecosystems? A review of nitrate removal pathways. Frontiers in Ecology and the Environment, 5(2): 89–96, doi: 10.1890/1540-9295(2007)5[89:HWOTRO]2.0.CO;2

Chambers L G, Osborne T Z, Reddy K R. 2013. Effect of salinity-altering pulsing events on soil organic carbon loss along an intertidal wetland gradient: a laboratory experiment. Biogeochemistry, 115(1–3): 363–383, doi: 10.1007/s10533-013-9841-5

Coble P G. 1996. Characterization of marine and terrestrial DOM in seawater using excitation-emission matrix spectroscopy. Marine Chemistry, 51(4): 325–346, doi: 10.1016/0304-4203(95)00062-3

Dekas A E, Fike D A, Chadwick G L, et al. 2018. Widespread nitrogen fixation in sediments from diverse deep-sea sites of elevated carbon loading. Environmental Microbiology, 20(12): 4281–4296, doi: 10.1111/1462-2920.14342

Galloway J N, Winiwarter W, Leip A, et al. 2014. Nitrogen footprints: past, present and future. Environmental Research Letters, 9(11): 115003, doi: 10.1088/1748-9326/9/11/115003

Gihring T M, Humphrys M, Mills H J, et al. 2009. Identification of phytodetritus-degrading microbial communities in sublittoral Gulf of Mexico sands. Limnology and Oceanography, 54(4): 1073–1083, doi: 10.4319/lo.2009.54.4.1073

Granger J, Sigman D M, Lehmann M F, et al. 2008. Nitrogen and oxygen isotope fractionation during dissimilatory nitrate reduction by denitrifying bacteria. Limnology and Oceanography, 53(6): 2533–2545, doi: 10.4319/lo.2008.53.6.2533

Hansen H P, Koroleff F. 1999. Determination of nutrients. In: Grasshoff K, Kremling K, Ehrhardt M, eds. Methods of Seawater Analysis. Weinheim: Wiley-VCH Verlag GmbH, 159–228

Harris D, Horwáth W R, Van Kessel C. 2001. Acid fumigation of soils to remove carbonates prior to total organic carbon or carbon-13 isotopic analysis. Soil Science Society of America Journal, 65(6): 1853–1856, doi: 10.2136/sssaj2001.1853

Hou Lijun, Wang Rong, Yin Guoyu, et al. 2018. Nitrogen fixation in the intertidal sediments of the Yangtze Estuary: occurrence and environmental implications. Journal of Geophysical Research: Biogeosciences, 123(3): 936–944, doi: 10.1002/2018JG004418

Huettel M, Berg P, Kostka J E. 2014. Benthic exchange and biogeochemical cycling in permeable sediments. Annual Review of Marine Science, 6: 23–51, doi: 10.1146/annurev-marine-051413-012706

Huettel M, Rusch A. 2000. Transport and degradation of phytoplankton in permeable sediment. Limnology and Oceanography, 45(3): 534–549, doi: 10.4319/lo.2000.45.3.0534

Ibánhez J S P, Leote C, Rocha C. 2011. Porewater nitrate profiles in sandy sediments hosting submarine groundwater discharge described by an advection-dispersion-reaction model. Biogeochemistry, 103(1–3): 159–180, doi: 10.1007/s10533-010-9454-1

Ibánhez J S P, Rocha C. 2014. Effects of recirculation of seawater enriched in inorganic nitrogen on dissolved organic carbon processing in sandy seepage face sediments. Marine Chemistry, 166: 48–58, doi: 10.1016/j.marchem.2014.09.012

Ibánhez J S P, Rocha C. 2016. Oxygen transport and reactivity within a sandy seepage face in a mesotidal lagoon (Ria Formosa, Southwestern Iberia). Limnology and Oceanography, 61(1): 61–77, doi: 10.1002/lno.10199

Ibánhez J S P, Rocha C. 2017. Kinetics of inorganic nitrogen turnover in a sandy seepage face on a subterranean estuary. Applied Geochemistry, 87: 108–121, doi: 10.1016/j.apgeochem.2017.10.015

Jafari S J, Moussavi G, Yaghmaeian K. 2015. High-rate biological denitrification in the cyclic rotating-bed biological reactor: Effect of COD/NO_3^-, nitrate concentration and salinity and the phylogenetic analysis of denitrifiers. Bioresource Technology, 197: 482–488, doi: 10.1016/j.biortech.2015.08.047

Janssen F, Huettel M, Witte U. 2005. Pore-water advection and solute fluxes in permeable marine sediments (II): benthic respiration at three sandy sites with different permeabilities (German Bight, North Sea). Limnology and Oceanography, 50(3): 779–792, doi: 10.4319/lo.2005.50.3.0779

Jiang Shan, Ibánhez J S P, Rocha C. 2018a. Influence of labile dissolved organic matter on nitrate reduction in a seepage face. Environmental Science and Pollution Research, 25(11): 10654–10667, doi: 10.1007/s11356-018-1302-1

Jiang Shan, Jin Jie, Zhang Guosen, et al. 2021. Nitrate in the Changjiang diluted water: an isotopic evaluation on sources and reaction pathways. Journal of Oceanology and Limnology, 39: 830–845, doi: 10.1007/s00343-020-0149-8

Jiang Shan, Kavanagh M, Rocha C. 2017b. Evaluation of the suitability of vacutainers for storage of nutrient and dissolved organic carbon analytes in water samples. Biology and Environment: Proceedings of the Royal Irish Academy, 177B: 33–46, doi: 10.3318/bioe.2017.01

Jiang Shan, Lu Haoliang, Liu Jingchun, et al. 2018b. Influence of seasonal variation and anthropogenic activity on phosphorus cycling and retention in mangrove sediments: a case study in China. Estuarine, Coastal and Shelf Science, 202: 134–144, doi: 10.1016/j.ecss.2017.12.011

Jiang Shan, Müller M, Jin Jie, et al. 2019. Dissolved inorganic nitrogen in a tropical estuary in Malaysia: transport and transformation. Biogeosciences, 16(14): 2821–2836, doi: 10.5194/bg-16-2821-2019

Jiang Shan, Su Yan, Lu Haoliang, et al. 2017a. Influence of polycyclic aromatic hydrocarbons on nitrate reduction capability in mangrove sediments. Marine Pollution Bulletin, 122(1–2): 366–375, doi: 10.1016/j.marpolbul.2017.06.076

Jiang Shan, Zhang Yixue, Jin Jie, et al. 2020. Organic carbon in a seepage face of a subterranean estuary: turnover and microbial interrelations. Science of the Total Environment, 725: 138220, doi: 10.1016/j.scitotenv.2020.138220

Jin Jie, Jiang Shan, Zhang Jing. 2020. Nitrogen isotopic analysis of nitrate in aquatic environment using cadmium-hydroxylamine hydrochloride reduction. Rapid Communications in Mass Spectrometry, 34(13): e8804, doi: 10.1002/rcm.8804

Jones R D, Hood M A. 1980. Effects of temperature, pH, salinity, and inorganic nitrogen on the rate of ammonium oxidation by nitrifiers isolated from wetland environments. Microbial Ecology, 6(4): 339–347, doi: 10.1007/BF02010496

Kuypers M M M, Marchant H K, Kartal B. 2018. The microbial nitrogen-cycling network. Nature Reviews Microbiology, 16(5): 263–276, doi: 10.1038/nrmicro.2018.9

Laverman A M, Canavan R W, Slomp C P, et al. 2007. Potential nitrate removal in a coastal freshwater sediment (Haringvliet Lake, The Netherlands) and response to salinization. Water Research, 41(14): 3061–3068, doi: 10.1016/j.watres.2007.04.002

Lawaetz A J, Stedmon C A. 2009. Fluorescence intensity calibration using the raman scatter peak of water. Applied Spectroscopy: 63(8), 936–940

Leote C, Epping E, Van Cappellen P. 2013. Phosphate sorption from seawater solutions: particle concentration effect. Marine Chemistry, 148: 52–62, doi: 10.1016/j.marchem.2012.12.002

Li Tao, Liu Sheng, Huang Liangmin, et al. 2011. Diatom to dinoflagellate shift in the summer phytoplankton community in a bay impacted by nuclear power plant thermal effluent. Marine Ecology Progress Series, 424: 75–85, doi: 10.3354/meps08974

Lin Gengming, Chen Yanghang, Huang Jiang, et al. 2020. Regional disparities of phytoplankton in relation to different water masses in the Northwest Pacific Ocean during the spring and summer of 2017. Acta Oceanologica Sinica, 39(6): 107–118, doi: 10.1007/s13131-019-1511-6

Magalhães C M, Joye S B, Moreira R M, et al. 2005. Effect of salinity and inorganic nitrogen concentrations on nitrification and denitrification rates in intertidal sediments and rocky biofilms of the Douro River estuary, Portugal. Water Research, 39(9): 1783–1794, doi: 10.1016/j.watres.2005.03.008

Marchant H K, Holtappels M, Lavik G, et al. 2016. Coupled nitrification–denitrification leads to extensive N loss in subtidal permeable sediments. Limnology and Oceanography, 61(3): 1033–1048, doi: 10.1002/lno.10271

Mariotti A, Germon J C, Hubert P, et al. 1981. Experimental determination of nitrogen kinetic isotope fractionation: Some principles; illustration for the denitrification and nitrification processes. Plant and Soil, 62(3): 413–430, doi: 10.1007/BF02374138

Marks B M, Chambers L, White J R. 2016. Effect of fluctuating salinity on potential denitrification in coastal wetland soil and sediments. Soil Science Society of America Journal, 80(2): 516–526, doi: 10.2136/sssaj2015.07.0265

Miao Yu, Liao Runhua, Zhang Xuxiang, et al. 2015. Metagenomic insights into salinity effect on diversity and abundance of denitrifying bacteria and genes in an expanded granular sludge bed reactor treating high-nitrate wastewater. Chemical Engineering Journal, 277: 116–123, doi: 10.1016/j.cej.2015.04.125

Nowicki B L. 1994. The effect of temperature, oxygen, salinity, and nutrient enrichment on estuarine denitrification rates measured with a modified nitrogen gas flux technique. Estuarine, Coastal and Shelf Science, 38(2): 137–156, doi: 10.1006/ecss.

1994.1009
O'Higgins T G, Wilson J G. 2005. Impact of the river Liffey discharge on nutrient and chlorophyll concentrations in the Liffey estuary and Dublin Bay (Irish Sea). Estuarine, Coastal and Shelf Science, 64(2–3): 323–334, doi: 10.1016/j.ecss.2005.02.025
Rao A M F, McCarthy M J, Gardner W S, et al. 2007. Respiration and denitrification in permeable continental shelf deposits on the South Atlantic Bight: rates of carbon and nitrogen cycling from sediment column experiments. Continental Shelf Research, 27(13): 1801–1819, doi: 10.1016/j.csr.2007.03.001
Rocha C. 1998. Rhythmic ammonium regeneration and flushing in intertidal sediments of the Sado estuary. Limnology and Oceanography, 43(5): 823–831, doi: 10.4319/lo.1998.43.5.0823
Rocha C. 2000. Density-driven convection during flooding of warm, permeable intertidal sediments: the ecological importance of the convective turnover pump. Journal of Sea Research, 43(1): 1–14, doi: 10.1016/S1385-1101(00)00002-2
Rocha C. 2008. Sandy sediments as active biogeochemical reactors: compound cycling in the fast lane. Aquatic Microbial Ecology, 53(1): 119–127, doi: 10.3354/ame01221
Rocha C, Forster S, Koning E, et al. 2005. High-resolution permeability determination and two-dimensional porewater flow in sandy sediment. Limnology and Oceanography: Methods, 3(1): 10–23, doi: 10.4319/lom.2005.3.10
Rocha C, Galvão H, Barbosa A. 2002. Role of transient silicon limitation in the development of cyanobacteria blooms in the Guadiana estuary, south-western Iberia. Marine Ecology Progress Series, 228: 35–45, doi: 10.3354/meps228035
Rocha C, Ibánhez J, Leote C. 2009. Benthic nitrate biogeochemistry affected by tidal modulation of Submarine Groundwater Discharge (SGD) through a sandy beach face, Ria Formosa, Southwestern Iberia. Marine Chemistry, 115(1–2): 43–58, doi: 10.1016/j.marchem.2009.06.003
Rocha C, Wilson J, Scholten J, et al. 2015. Retention and fate of groundwater-borne nitrogen in a coastal bay (Kinvara Bay, Western Ireland) during summer. Biogeochemistry, 125(2): 275–299, doi: 10.1007/s10533-015-0116-1
Santoro A E. 2010. Microbial nitrogen cycling at the saltwater–freshwater interface. Hydrogeology Journal, 18(1): 187–202, doi: 10.1007/s10040-009-0526-z
Santoro A E, Boehm A B, Francis C A. 2006. Denitrifier community composition along a nitrate and salinity gradient in a coastal aquifer. Applied and Environmental Microbiology, 72(3): 2102–2109, doi: 10.1128/AEM.72.3.2102-2109.2006
Santos I R, Eyre B D, Glud R N. 2012. Influence of porewater advection on denitrification in carbonate sands: evidence from repacked sediment column experiments. Geochimica et Cosmochimica Acta, 96: 247–258, doi: 10.1016/j.gca.2012.08.018
Schulp J A, Stouthamer A H. 1970. The influence of oxygen, glucose and nitrate upon the formation of nitrate reductase and the respiratory system in *Bacillus licheniformis*. Microbiology, 64(2): 195–203, doi: 10.1099/00221287-64-2-195
Seitzinger S P. 1987. Nitrogen biogeochemistry in an unpolluted estuary: the importance of benthic denitrification. Marine Ecology Progress Series, 41: 177–186, doi: 10.3354/meps041177
Sigman D M, Casciotti K L, Andreani M, et al. 2001. A bacterial method for the nitrogen isotopic analysis of nitrate in seawater and freshwater. Analytical Chemistry, 73(17): 4145–4153, doi: 10.1021/ac010088e
Silva L C F, Lima H S, Sartoratto A, et al. 2018. Effect of salinity in heterotrophic nitrification/aerobic denitrification performed by acclimated microbiota from oil-produced water biological treatment system. International Biodeterioration & Biodegradation, 130: 1–7, doi: 10.1016/j.ibiod.2018.03.009
Song Guodong, Liu Sumei, Marchant H, et al. 2013. Anaerobic ammonium oxidation, denitrification and dissimilatory nitrate reduction to ammonium in the East China Sea sediment. Biogeosciences, 10(3): 4671–4710, doi: 10.5194/bgd-10-4671-2013
Song Z F, An J, Fu G H, et al. 2011. Isolation and characterization of an aerobic denitrifying *Bacillus* sp. YX-6 from shrimp culture ponds. Aquaculture, 319(1–2): 188–193, doi: 10.1016/j.aquaculture.2011.06.018
Stedmon C A, Bro R. 2008. Characterizing dissolved organic matter fluorescence with parallel factor analysis: a tutorial. Limnology and Oceanography: Methods, 6(11): 572–579, doi: 10.4319/lom.2008.6.572
Stubbins A, Lapierre J F, Berggren M, et al. 2014. What's in an EEM? Molecular signatures associated with dissolved organic fluorescence in boreal Canada. Environmental Science & Technology, 48(18): 10598–10606, doi: 10.1021/es502086e
Sun Dongyao, Tang Xiufeng, Zhao Mengyue, et al. 2020. Distribution and diversity of comammox *Nitrospira* in coastal wetlands of China. Frontiers in Microbiology, 11: 589268, doi: 10.3389/fmicb.2020.589268
Verma A, Barua A, Ruvindy R, et al. 2019. The genetic basis of toxin biosynthesis in dinoflagellates. Microorganisms, 7(8): 222, doi: 10.3390/microorganisms7080222
Wang Yongfeng, Gu Jidong. 2014. Effects of allylthiourea, salinity, and pH on ammonia/ammonium-oxidizing prokaryotes in mangrove sediment incubated in laboratory microcosms. Applied Microbiology and Biotechnology, 98(7): 3257–3274, doi: 10.1007/s00253-013-5399-3
Wang Yu, Ye Fei, Wu Shengjun, et al. 2020. Biogeographic pattern of bacterioplanktonic community and potential function in the Yangtze River: roles of abundant and rare taxa. Science of the Total Environment, 747: 141335, doi: 10.1016/j.scitotenv.2020.141335
Weigand M A, Foriel J, Barnett B, et al. 2016. Updates to instrumentation and protocols for isotopic analysis of nitrate by the denitrifier method. Rapid Communications in Mass Spectrometry, 30(12): 1365–1383, doi: 10.1002/rcm.7570
Weston N B, Giblin A E, Banta G T, et al. 2010. The effects of varying salinity on ammonium exchange in estuarine sediments of the Parker River, Massachusetts. Estuaries and Coasts, 33(4): 985–1003, doi: 10.1007/s12237-010-9282-5
Wilson J, Rocha C, Coxon C. 2016. Combining Earth Observation and Geochemical Tracing Techniques for Groundwater Detection and Evaluation in Ireland. Wexford, Ireland: EPA Research
Yang Bin, Liu Sumei, Zhang Guoling. 2018. Geochemical characteristics of phosphorus in surface sediments from the continental shelf region of the northern South China Sea. Marine Chemistry, 198: 44–55, doi: 10.1016/j.marchem.2017.11.001
Yoshie S, Noda N, Tsuneda S, et al. 2004. Salinity decreases nitrite reductase gene diversity in denitrifying bacteria of wastewater treatment systems. Applied and Environmental Microbiology, 70(5): 3152–3157, doi: 10.1128/AEM.70.5.3152-3157.2004
Zhou Minghua, Butterbach-Bahl K, Vereecken H, et al. 2017. A meta-analysis of soil salinization effects on nitrogen pools, cycles and fluxes in coastal ecosystems. Global Change Biology, 23(3): 1338–1352, doi: 10.1111/gcb.13430

Supplementary information:

Table S1. Mean concentrations of DO, DOC, DIN species and SRP at input solutions in each group

Fig. S1. The predicted functional profiles (different functions levels; Wang et al., 2020) of the sampling sediment in the Dublin Bay. The number indicates the relative abundance for each function (total abundance, 1).

The supplementary information is available online at https://doi.org/10.1007/s13131-021-1811-5. The supplementary information is published as submitted, without typesetting or editing. The responsibility for scientific accuracy and content remains entirely with the authors.